ISBN: 978-3-95450-233-2 ISSN: 2673-5504 doi:10.18429/JACoW-SRF2021-SUPTEV006

COMMISSIONING OF A CALIBRATION DEVICE FOR SECOND SOUND QUENCH DETECTION

L. Ebeling[1*], W. Hillert[1], D. Reschke, L. Steder, DESY, Hamburg, Germany
[1]also at Universität Hamburg, Germany

Abstract

An important part of research and development in the field of superconducting radio frequency technology is the quench detection since these breakdowns of superconductivity often limit the cavity performance. Although the second sound based quench detection is widely used, only few studies dealing with its systematic uncertainties exist. Hence, the vertical test stands at the cavity test facility of DESY were extended by calibration device prototypes in order to estimate the accuracy of this method. For the first time at DESY, artificial signals have been generated and reconstructed by heating power film resistors. These second sound signals are determined using noise canceling algorithms and the existing reconstruction software. To evaluate the reconstructed positions, the absolute distance between reconstructed and true coordinates is calculated. Thus, a first uncertainty map of the cavity surface is created to quantify the reconstruction results of actual cavity quenches including systematic effects of the quench positioning like the varying sensor coverage around the cavity.

SECOND SOUND BASED QUENCH DETECTION

Superconducting radio frequency (SRF) cavities made of niobium play a pivotal role in particle acceleration, but their performance is often limited by quenches. These local breakdowns of superconductivity are mainly caused by exceeding the critical temperature or the critical magnetic field of the material.

Due to the heat dissipation during a quench, a temperature-driven entropy wave is generated which propagates through the liquid helium used to cool the cavity. These so-called second sound signals are detected by oscillating superleak transducers (OSTs) [1] based on a capacitor microphone. Utilizing the running times of the detected second sound signals, the wave origin (quench) is reconstructed via trilateration [2] or ray-tracing [3] algorithms.

In order to quantify the reconstruction quality of the second sound method, a device for external calibration was commissioned. As a summary of a recently finished bachelor thesis [4], the commissioning and the calibration results are presented in the following.

At DESY, the quench localization based on second sound waves is performed in vertical test stands. First, the cavity is mounted into an insert supporting up to 16 OSTs. As shown in Fig. 1, four layers of sensors are attached at four metal rods around the cavity.

Within the cryostats, the insert (including the cavity and sensors) is then cooled with liquid helium to a temperature of about 1.8 K. As helium partly condensates into its superfluid state below the lambda-point of 2.17 K, the propagtion of second sound waves is enabled.

Figure 1: Oscillating superleak transducers (here with white cover caps) mounted on an insert supporting a TESLA-shape single cell SRF cavity with a resonant frequency of 1.3 GHz.

The OSTs consist of a capacitor with parallel plates; one rigid and the other flexible and porous. Whereas the superfluid He-II can pass the porous membrane due to its vanishing viscosity, the normal fluid He-I is blocked and exerts pressure onto the flexible plate during a second sound wave [1]. This causes a shift of the capacitor plates distance and changes thereby its capacity. Since the charge is held constant, the change of capacity is measured via the amplified voltage across the OST.

TRILATERATION ALGORITHM FOR QUENCH RECONSTRUCTION

Using the already existing reconstruction software [2], the quench spot is located via trilateration based on the running times between the signal generation and its detection by OSTs in direct line of sight to the wave origin. In order to locate the quench position in three dimensions, three or more

* lukas.ebeling@desy.de

ISBN: 978-3-95450-233-2 ISSN: 2673-5504 doi:10.18429/JACoW-SRF2021-SUPTEV006

sensors with at least two different angular coordinates must be used.

Since the quench location is not measured directly, further assumptions about the quench area and the second sound propagation have to be made. For an analysis based on trilateration, the duration of the cavity quench is presumed to be much shorter than the second sound propagation time. Secondly, the quench spot itself is supposed to be in good approximation point-like.

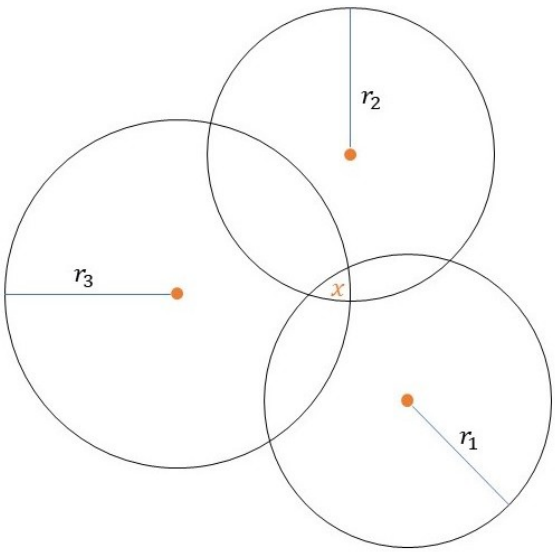

Figure 2: Schematic diagram of trilateration algorithm. Reconstructed quench spot **x** corresponds to the intersection of imaginary spheres centered at the sensor coordinates.

As shown in Fig. 2, the quench spot is then located by finding the intersection of spheres centered at the n used sensors. Their radii correspond to the second sound propagation distances r_i which are calculated from the signal running times t_i and the second sound velocity u_2 [5]:

$$r_i = t_i \cdot u_2. \tag{1}$$

The trilateration approach is implemented by minimizing the root-mean-square error (RMSE) of the propagation distances r_i and the theoretical distances D_i (explained below) as a function of the unknown quench spot **x**:

$$RMSE(\mathbf{x}) = \sqrt{\sum_{i=0}^{n} \frac{(D_i(\mathbf{x}) - r_i)^2}{n}}. \tag{2}$$

The theoretical distances D_i between a potential quench spot **x** and the different OST positions $\mathbf{p}_i$ are determined as follows:

$$D_i(\mathbf{x}) = |\mathbf{x} - \mathbf{p}_i|. \tag{3}$$

In conclusion, a quench spot minimizing the RMSE, minimizes the difference between the propagation distances and the theoretical distances to the sensors.

Utilizing this algorithm, the quench spot is first determined in Cartesian coordinates with a coordinate origin lying on the beam axis within the cavity cell (equator height). The software then translates the position into cylindrical coordinates r, α^* and z (cf. Fig. 4) relative to the cavity. For technical reasons, the cavity is often mounted into the insert with a rotation angle. However, since the sensor coverage discussed later depends on the angular coordinate α in the reference frame of the insert, the angular coordinate α^* must be transformed with the help of this rotation angle.

CALIBRATION TOOL SETUP

Simulating the heat dissipation of a cavity quench, second sound signals can also be generated by different heat sources. Studies in this field [6] show that such heaters can be realized with ohmic resistors due to their efficient conversion of electric energy to heat. The resistors are placed at well-known coordinates and heated by applying short electrical pulses to emit a second sound signal. Analogous to the signals generated by a cavity quench, these artificial waves are detected, reconstructed, and evaluated using the same sensors and reconstruction methods. By comparing the reconstructed and actual coordinates of the resistors, systematic studies of the reconstruction algorithms and the sensor positioning become possible.

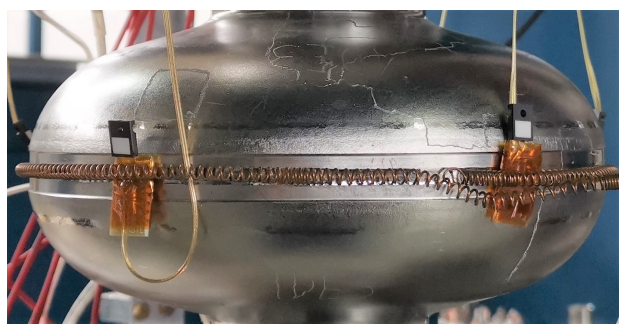

Figure 3: Power film resistors MP915 with about 50 Ω connected to flat ribbon cables. Contacts insulated from the cavity by Kapton® tape. White heat dissipating surface [7] turned towards surrounding OSTs.

In order to mimic the typical path of second sound signals, resistors are attached at different angles around the cavity equator, as depicted in Fig. 3. Based on preliminary performance tests, power film resistors [7] with a resistance of about 50 Ω are heated by electric pulses with a voltage of about 30 V and a duration of 0.1 s.

Pulse Generation Device

The resistors of the calibration tool are connected to a pulse generation device via flat ribbon cables and a feedthrough of the cryostat. This device relies on two circuits operating on different voltage levels [4]. A timer in the first circuit is powered by a battery within the device. Once a button on the front panel is pressed, it generates a control pulse with small amperage. While this control current is

ISBN: 978-3-95450-233-2 ISSN: 2673-5504 doi:10.18429/JACoW-SRF2021-SUPTEV006

applied to a transistor in the second circuit, the connected external resistor is powered by an external power supply.

Introducing ΔD

Using the calibration device for artificial generation of second sound waves, the wave origin is well-known. Hence, the reconstruction quality can be quantified by the total distance ΔD between the true position $\mathbf{x}_{true}$ and the reconstructed coordinates $\mathbf{x}_{recon}$. It is calculated using the Euclidean vector norm:

$$\Delta D = |\mathbf{x}_{recon} - \mathbf{x}_{true}| \tag{4}$$

The true position $\mathbf{x}_{true}$ of a resistor is defined as the center of its heat dissipating surface, as these white ceramic windows are presumed to be the origin of the artificially generated second sound waves. This assumption was validated by reconstructing the positions of differently oriented resistors [4]. The uncertainties of ΔD are calculated via Gaussian error propagation for uncorrelated parameters based on the uncertainty of measuring $\mathbf{x}_{true}$ using a folding rule and an angle disc [4].

SYSTEMATIC EFFECT OF SENSOR COVERAGE

By assuming that each OST covers an angle of 120° of the cavity equator [2], the sensor coverage depicted in Fig. 4 is estimated. According to this estimation, two areas with reduced sensor coverage are suspected around the angles of 170° and 350°.

Within these so-called blind areas, a direct line of sight can only be drawn to sensors with an identical angular coordinate mounted at the same supporting rod. Since the reconstruction algorithm requires sensors with at least two different angular coordinates, however, OSTs without a direct line of sight have to be included in these regions. Thus, large distortions of the reconstruction are expected.

Resistors mounted within these blind regions lead, as expected, to reconstructions with large ΔD-values indicating a distortion of up to 33.6 mm. An exemplary reconstruction of a resistor placed at an angle of 186° is shown in Fig. 5. The reconstructed position of this film resistor exhibits a much shorter radius relative to the cavity center. Thus, its position is not reconstructed on the cavity surface, but rather within the cavity cell. Other resistors within blind areas at angles of 172° and 330° produce similar results.

Note that the scope of the fully covered and blind areas has only been estimated. Hence, one resistor at an angle of 31°, for example, was reconstructed with a small ΔD-value of 6.0 mm ± 1.0 mm even outside the estimated areas with full sensor coverage. This suggests that assuming the same cover angle of 120° for all sensors, despite differing distances of the OSTs to the cavity equator (cf. Fig. 4), is too simplistic. By placing more film resistors at the transition regions, the actual angular extent of blind and fully covered areas will be investigated in the future.

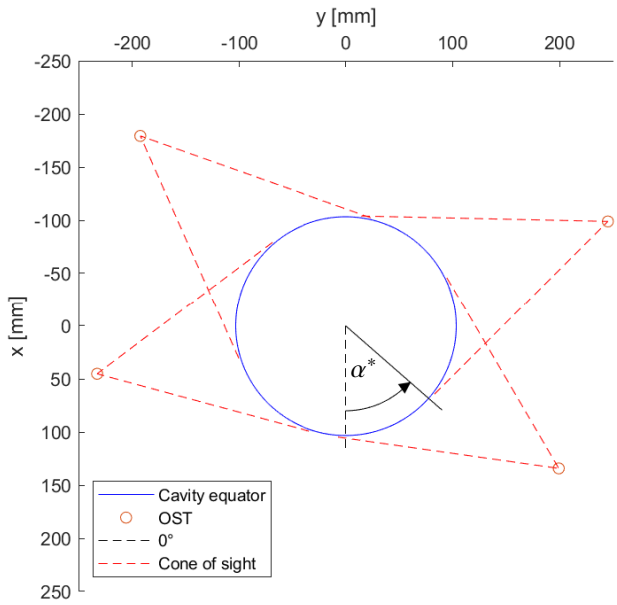

Figure 4: Sensor coverage of the cavity surface at the equator shown in top view. The angular coordinate α^* of a quench runs counterclockwise starting at the cavity front.

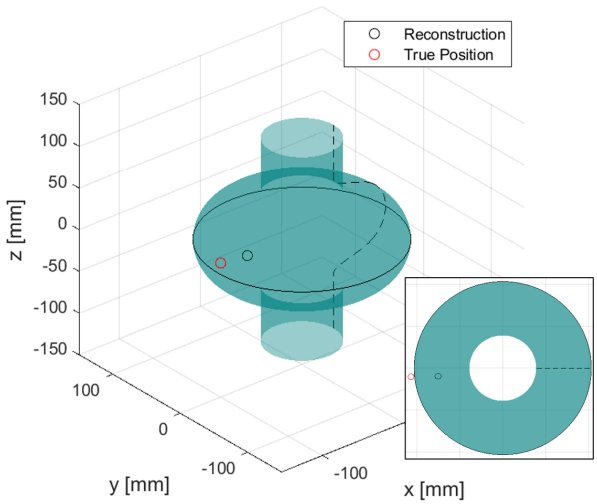

Figure 5: Reconstruction of a resistor attached to the cavity at about 186° in perspective view and top view. Reconstruction yields a ΔD-value of 33.6 mm ± 1.3 mm.

In order to improve the reconstruction quality in regions with reduced sensor coverage, the insert has to be extended by additional supporting rods at angles of about 0° and 180° equipped with more sensors.

ANGULAR DISTRIBUTION OF ΔD

At a total of eight different angles around the equator, power film resistors were attached and heated by means of short electric pulses. The artificially generated second sound signals are reconstructed using the trilateration algorithm yielding the angular distribution of ΔD (deviation from true position) shown in Fig. 6.

ISBN: 978-3-95450-233-2 ISSN: 2673-5504 doi:10.18429/JACoW-SRF2021-SUPTEV006

As expected, the smallest ΔD-values are achieved within fully covered areas (black markers) at angles of about 100° and 300°. Resistors mounted within blind regions (red markers) lead, on the other hand, to reconstructions with distortions of up to 33.6 mm. Note that every angular coordinate corresponds to three to four ΔD-values, since the power film resistors were heated three to four times at every position. In summation, the systematic effects of the sensor coverage are clearly captured by strongly varying ΔD-values.

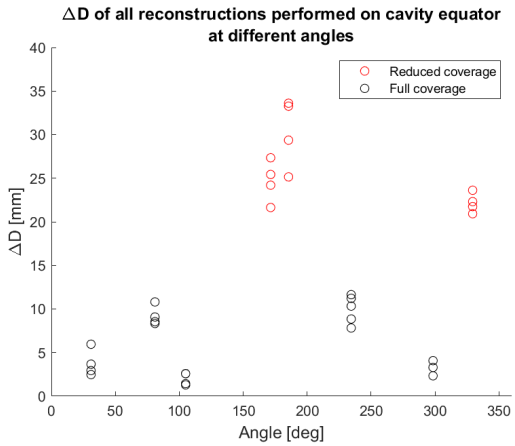

Figure 6: ΔD-values of all reconstructions performed with calibration tool plotted against the angular coordinate of the resistors true position. Areas with reduced sensor coverage highlighted in red.

As an essential result of the calibration tool investigation, a first ΔD-map of the cavity insert (at equator height) was created presented in the table below. Although ΔD cannot be calculated for cavity quenches (true position is unknown), the reconstructed coordinates can be compared to the varying regions of the ΔD-map. Thus, an estimation of the reconstruction quality of actual quenches is enabled.

Table 1: ΔD-map of Cavity Equator

angle [deg]	coverage	ΔD_{max} [mm]
31	fully covered	6.0 ± 1.0
81	fully covered	10.8 ± 2.2
105	fully covered	2.6 ± 1.1
172	reduced	27.3 ± 1.3
186	reduced	33.6 ± 1.3
235	fully covered	11.6 ± 2.0
299	fully covered	4.1 ± 3.0
330	reduced	23.6 ± 1.2

After reconstructing the quench position $\mathbf{x}_{recon}$ within the reference frame of the insert, it is compared to the specified angles of the ΔD-map. Using the ΔD-value of the corresponding region, the reconstruction quality is quantified. Note that in every region the maximal ΔD-value was taken into account as a worst-case estimation.

With this ΔD-map already at hand, a substantial tool for reconstruction analysis has been developed in the scope of these studies. In the future, the calibration device will be used to create an even more detailed map of the inserts at DESY.

COMPARISON OF ΔD AND RMSE

For cavity quenches, the minimized root-mean-square error of the trilateration algorithm was so far considered as an indicator of the reconstruction quality. In the following, the systematic effects of the varying sensor coverage on the RMSE are discussed and compared to the influence on ΔD. In Fig. 7, RMSE and ΔD of all reconstructions of the calibration tool are shown, with red markers indicating areas with reduced sensor coverage.

With respect to ΔD, clear differences of the reconstruction quality caused by the sensor coverage are apparent. Such systematic effects, however, are not reflected by the RMSE. In contrast to all expectations, the position of resistors attached at blind spots are even reconstructed with smaller RMSE-values on average. Apart from areas with reduced sensor coverage, the root-mean-square errors are uniformly distributed between 0 mm and 3.7 mm. The maximum values of RMSE and ΔD of 3.7 mm and 33.6 mm ± 1.3 mm, respectively, also reveal significant differences in the range of both measures.

Overall, no correlation of RMSE and ΔD can be determined. Accordingly, it is recommended to evaluate the reconstruction results based on the introduced ΔD-map instead of the RMSE.

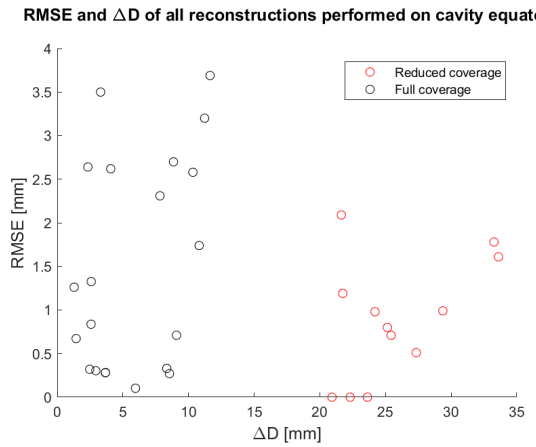

Figure 7: RMSE and ΔD-values of all reconstructions obtained by using the calibration tool plotted against each other. Areas with reduced sensor coverage highlighted in red.

CONCLUSION

During these studies, the existing second sound test facility at DESY was expanded by calibration tool prototypes. Constructed based on power film resistors, these devices generate artificial second sound signals after being heated by short electrical pulses. The film resistors were attached at

ISBN: 978-3-95450-233-2 ISSN: 2673-5504 doi:10.18429/JACoW-SRF2021-SUPTEV006

several angles around the cavity equator to mimic the usual path of quench induced signals, including a typical sensor positioning.

Analogous to quench spots, the coordinates of these resistors were reconstructed based on trilateration. As an estimation of the reconstruction quality, ΔD was introduced, reflecting the total distance between the reconstructed and true coordinates of a resistor. Thus, already presumed regions with reduced sensor coverage have been confirmed by large ΔD-values.

Although very large root-mean-square errors of the trilateration algorithm may indicate an insufficient signal quality, no correlation between RMSE and ΔD could be observed. In addition, systematic effects of the sensor coverage are not reflected by the RMSE. Thus, the RMSE should only be considered as a quality estimate with caution.

Finally, the calibration tool prototypes were used to create a first ΔD-map of the differently covered areas around the cavity surface. As a worst-case estimation, the highest ΔD-values were considered for each measured angle. Using these maximal ΔD-values at the corresponding coordinates, the reconstruction quality of actual cavity quenches can be evaluated from now on using this ΔD-map.

NEXT STEPS

In order to improve the reconstruction quality in areas with reduced sensor coverage in the future, the insert has to be extended by additional supporting rods at angles of about 0° and 180° equipped with more sensors. Afterwards a more granular ΔD-map will be created with the help of the introduced calibration tool. In addition, more accurate mounting methods for attaching the resistors are being investigated.

ACKNOWLEDGMENTS

This work was supported by the Helmholtz Association within the topic Accelerator Research and Development (ARD) of the Matter and Technologies (MT) Program. Special thanks goes to Carsten Müller and his colleagues of the electronic laboratory. They provided electrical components and tools such as the pulse generation device and supported the assembling of a calibration tool.

REFERENCES

[1] Z. A. Conway, D. L. Hartill, H. Padamsee, and E. N. Smith, "Defect Location in Superconducting Cavities Cooled with He-II Using Oscillating Superleak Transducers," in *Proc. 23rd Particle Accelerator Conf. (PAC'09)*, Vancouver, Canada, May 2009, paper TU5PFP044, pp. 921–923.

[2] Bosse Bein, "Systematic studies of a cavity quench localization system," Master thesis, University Hamburg, Hamburg, Germany, 2019. https://bib-pubdb1.desy.de/record/422834/files/MasterThesis_B_Bein.pdf

[3] Y. Tamashevich, "Diagnostics and treatment of 1.3 GHz Nb cavities," Ph.D. thesis, University Hamburg, Hamburg, Germany, 2016.

[4] L. Ebeling, "Commissioning of a Calibration Device for Second Sound Based Quench Detection and Reconstruction Analysis," Bachelor thesis, University Hamburg, Hamburg, Germany, 2021.

[5] R. J. Donelly and C. F. Barenghi, "The Observed Properties of Liquid Helium at the Saturated Vapor Pressure," *Journal of Physical and Chemical Reference Data,* vol. 27, no 6, pp.1217-1274, 1998. doi:10.1063/1.556028

[6] M. Fouaidy *et al.*, "Calibration and Characterization of Capacitive OST Quench Detectors in SRF Cavities at IPN Orsay," in *Proc. 16th Int. Conf. RF Superconductivity (SRF'13)*, Paris, France, Sep. 2013, paper TUP103, pp. 714–718.

[7] *High Performance Film Resistors,* CADDOCK Electronics, Inc., http://www.caddock.com/Online_catalog/Mrktg_Lit/MP9000_Series.pdf